Journal of Magnetic Resonance **141,** 239–255 (1999)
Article ID jmre.1999.1905, available online at http://www.idealibrary.com on IDEAL®

Calculations of Multipulse Sequence in NQR of Spins $\frac{3}{2}$

Christophe Odin

Groupe Matière Condensée et Matériaux, UMR 6626 au CNRS, Université Rennes I, Campus de Beaulieu, 35042 Rennes Cedex, France

Received February 17, 1999; revised August 2, 1999

The general formalism of the interaction representation with respect to an operator which is its own inverse is developed and applied to pure NQR of spins $I = \frac{3}{2}$. Under the assumption of no relaxation and no dipolar coupling, it is shown that the calculation of the response to pure NQR multipulse sequences can be performed with the same concepts used in high field NMR, such as coherence pathways. All the tools and mathematical expressions to predict the time evolution of the signal created by a pure NQR multipulse sequence are presented explicitly. It takes into account the off-resonance irradiation as well as the angular dependence of the excitation and detection for every value of the electric field gradient asymmetry parameter. Particular attention is devoted to the powder average, which is performed via a probability function derived analytically for the first time, leading to a drastic reduction of simulation times. The theory is illustrated by the study of the optimization and excitation bandwidths of one- to three-pulse sequences and compared to experimental results on Chloranil. We show that the three-pulse "stimulated echo" sequence gives a more uniform excitation profile than the traditional two-pulse echo sequence for powder samples. Thus, the "stimulated echo" sequence could be useful to cover a large spectrum when the experiment duration, or the signal to noise ratio, are not critical parameters. Analytical expressions for the nutation spectra obtained by one or two-pulse sequences are also derived for the first time.

Key Words: **NQR; quadrupolar nuclei; interaction representation formalism; excitation bandwidth; powder average; nutation spectra.**

INTRODUCTION

All nuclei with a spin $I \geq 1$ possess a quadrupolar moment M_Q, which can interact with the electric field gradient (EFG) $V_{\alpha\beta} = (\partial^2 V/\partial\alpha\partial\beta)$ evaluated at the nuclear site, provided the site point symmetry is lower than cubic. The corresponding quadrupolar interaction energy of the nuclear charge distribution with the EFG is proportional to the product $M_Q \cdot (V_{\alpha\beta})$. The EFG tensor $(V_{\alpha\beta})$ strongly reflects the symmetry of the site and provides a concise summary of the nature of the charge environment of the nucleus (electronic cloud distortion, crystal field, etc.). This makes the quadrupolar interaction a unique probe to study any physical phenomena affecting the charge distribution around a nucleus, as for example phase transitions, superconductivity, and incommensurability. Among the experimental techniques available to measure the quadrupolar interaction, magnetic resonance spectroscopy techniques are particularly appealing because of their large and usually simple applicability. Moreover, one can have access to a large range of time scales, an important feature in the study of phase transitions or of disordered systems.

Depending on the strength of the quadrupolar interaction $M_Q \cdot (V_{\alpha\beta})$ compared to the Zeeman interaction γB, where γ is the nuclear gyromagnetic ratio, and B is the external applied static magnetic field, magnetic resonance techniques can be divided into two limit cases: the high field extreme of nuclear magnetic resonance (NMR) when the Zeeman splitting dominates the quadrupolar interaction (and usually also dominates the other terms in the Hamiltonian such as chemical shift and spin–spin interactions) or the low field limit of Nuclear Quadrupolar Resonance (NQR) when the quadrupolar interaction is predominant. The so-called *pure* NQR designation being used when no external static magnetic field is present (except of course the Earth's magnetic field). In both limits, one can make use of perturbation theory to calculate the energy spectrum, which usually leads to severe simplifications of the formalism, whereas the intermediate case $M_Q \cdot (V_{\alpha\beta}) \sim \gamma B$ could only be solved numerically to our knowledge.

Unlike NMR, the main drawback of NQR is that the frequency of the nucleus is not known since it specifically depends on the nuclear environment. Once the frequency is found, its variation with external parameters such as temperature are almost directly proportional to the variation of the effective EFG. An important difference between NQR and NMR should be stressed. In NMR, the quadrupolar resonance frequencies $\omega_Q(\theta, \varphi)$ depend on the polar angles relative to the orientations of the principal axis system (PAS) of the EFG at the nucleus with respect to the laboratory frame (*1–3*). As a consequence, the components of the tensors can be determined by the analysis of rotation patterns about two or three axes of a single crystal. In powder or polycrystalline samples, the interpretation of the spectra is complicated because the line broadening comes from all the contributions of the different crystallites, possibly convoluted by a distribution of environments, chemical shift, and dipolar interactions. Moreover, the excitation profile of a radiofrequency (RF) pulse in NMR may

1090-7807/99 $30.00

be strongly distorted if the quadrupolar interaction couldn't be neglected compared to the RF power ("soft pulse").

Rotations patterns are also observed in NQR when a small static field is applied to remove the degeneracy of the energy levels. The particularity of pure NQR is that the spatial symmetry is broken only during the pulses by the application of the RF field. Whereas the frequency of a given site remains constant, both the excitation and the reception of the signal are affected by the relative orientation of the emitting/receiving coil with respect to the PAS of the EFG at the nucleus under study, modulating both the nutation frequencies of the isochromats and the signal amplitude. Therefore, in pure NQR, it is the amplitude of the signal which is angular dependent. In contrast to NMR, the line broadening in pure NQR would only reflect the distribution of EFG (neglecting dipolar broadening and the residual external magnetic fields).

In this article, our main concern is pure NQR of spin $I = \frac{3}{2}$. Much work has been devoted to calculate the NQR response of spin $I = \frac{3}{2}$ systems to strong radiofrequency pulses, using different formalisms. The earlier descriptions were based on the solution of the time-dependent Schrödinger equation (see for instance (*4*)). More recently introduced was a tensor operator formalism (*5, 6*) or a spin $\frac{1}{2}$ description of spins $\frac{3}{2}$ (*7*). Other descriptions using the full matrices were described (*8, 9*), as well as iterative procedure based on the evaluation of the Baker–Campbell–Hausdorff series with computer programs like MAPLE (*10*). However, to our knowledge, the most used formalism seems to be the interaction representation introduced by Pratt (*11, 12*), since operational calculations using the density-matrix could be performed. As an example, the nutation experiment introduced by Harbison *et al.* (*13*) to measure the asymmetry parameter η was calculated on such grounds (*14*), as well as NQR imaging multipulse sequences (*15*). Subjects, such as the study of incommensurate phases, or superconducting materials, show very broad NQR spectra, which are not excited totally by a single echo pulse sequence. Recently, a procedure to rebuild spectra based on a two-pulse echo sequence appeared (*16*). A question which arises is whether more complicated sequences using three pulses or more could enlarge the frequency selectivity. Therefore, a good understanding of the properties of multipulse sequences is needed.

The aim of this work is to present another derivation of the interaction representation of pure NQR of spins $I = \frac{3}{2}$ based on the fact that the square of the pure quadrupolar Hamiltonian of a spin $I = \frac{3}{2}$ is in fact proportional to the identity matrix. Section I introduces the Hamiltonians and tools needed in the study of NQR, whereas Section II presents the general form of the matrices in the representation interaction of an operator which is its own inverse as well as their main properties. The application of this framework to the case of pure spin $\frac{3}{2}$ NQR in Section III greatly simplifies the calculations leading to a full analogy with the high field NMR formalism. It is shown that pure spin $\frac{3}{2}$ NQR multipulse sequences can be calculated in the same way as the NMR response of a single spin of arbitrary value I to an Hamiltonian including the frequency offset and the radiofrequency excitation. All useful formula are described extensively. Section IV is completely devoted to the problem of the powder average. An analytical expression for the probability function of the angular factor affecting the effective nutation angle of the isochromats and the amplitude of the signal is derived for the first time, which leads us to propose a drastic simplification of the powder average procedure. Section V then illustrates the calculations schemes proposed in Sections III and IV with some applications concerning the optimization and the frequency response profile of one- to three-pulse sequences, and the shape of nutation spectra obtained from one- or two-pulse sequences. Simulations are compared with experiments performed on Chloranil at ambient temperature.

I. QUADRUPOLAR INTERACTION OF A SPIN I = $\frac{3}{2}$

The Hamiltonian of a single $I \geq 1$ spin may be decomposed into four contributions: the pure quadrupolar Hamiltonian H_q, a Zeeman Hamiltonian H_Z, a dipolar Hamiltonian H_d if the spin is coupled to other spins, and, when the sample is irradiated by a radiofrequency field (RF), the RF Hamiltonian H_{RF} (*1–3*). The NQR domain considers that the norm of the quadrupolar Hamiltonian is much larger than the norms of the three other contributions. In the following, we only deal with the pure NQR case (no magnetic field applied) and neglect the dipolar interactions as well as all relaxation phenomena.

In NQR, it is more suited to quantify the spin operators $\{I_x, I_y, I_z\}$ in the principal axis system of the EFG at the nucleus under study, the z axis being oriented along the direction of the highest eigenvalue in absolute value. Within this convention, the Cartesian representation of the pure quadrupolar part of the Hamiltonian of a spin $I = \frac{3}{2}$ nucleus of quadrupole moment M_Q is then (*2*)

$$H_q = \frac{1}{6}\frac{eM_Q V_{zz}}{2}\left\{3I_z^2 - \frac{15}{4} + \frac{\eta}{2}\left(I_+^2 + I_-^2\right)\right\}, \qquad [1]$$

where

$$\eta = \frac{V_{xx} - V_{yy}}{V_{zz}} \qquad [2]$$

is the asymmetry parameter.

The EFG tensor ($V_{\alpha\beta}$) is defined as the second spatial derivatives of the classical electrostatic potential V at the nucleus site: $V_{\alpha\beta} = (\partial^2 V/\partial\alpha\partial\beta)$, where the subscripts α and β indicate x, y, or z components. This tensor is symmetric and traceless. Therefore, the two numerical parameters η and eq = V_{zz} are sufficient to characterised the EFG tensor. The values of η could be restricted to the interval $0 \leq \eta \leq 1$ with the

convention $|V_{xx}| \leq |V_{yy}| \leq |V_{zz}|$. Physically, the asymmetry parameter gives a measure of the departure of the EFG from axial symmetry.

In the following, the Hamiltonian are expressed in units of angular frequencies ($\hbar = 1$). The raising and lowering operators $\{I_+, I_-\}$ are, as usual $I_\pm = I_x \pm iI_y$.

The pure quadrupolar Hamiltonian H_q has two opposite twofold eigenvalues

$$\pm \frac{e^2 q M_Q}{4} a, \qquad [3]$$

where

$$a = \sqrt{1 + \frac{\eta^2}{3}}. \qquad [4]$$

The corresponding NQR transition angular frequency is

$$\omega_q = \frac{e^2 q M_Q}{2} a. \qquad [5]$$

A straightforward calculation shows that H_q may be rewritten as

$$H_q = \frac{\omega_q}{2} Q, \qquad [6]$$

where Q has the interesting property that it is its own inverse, that is

$$Q^2 = I_4, \qquad [7]$$

where I_n will design in the following the $n \times n$ identity matrix.

In fact, the result that the square of H_q is proportional to the identity matrix is a direct consequence of the Cayley–Hamilton theorem (*17*), since H_q has only two opposite twofold eigenvalues.

In the basis of the eigenvalues of I_z $\{\frac{3}{2}, \frac{1}{2}, -\frac{1}{2}, -\frac{3}{2}\}$, the matrix representation of Q is

$$Q = \frac{1}{3a} \begin{pmatrix} 3 & 0 & \eta\sqrt{3} & 0 \\ 0 & -3 & 0 & \eta\sqrt{3} \\ \eta\sqrt{3} & 0 & -3 & 0 \\ 0 & \eta\sqrt{3} & 0 & 3 \end{pmatrix}. \qquad [8]$$

In order to simplify the calculation of matrix products, all the matrices will be represented by a sum of Kronecker products of spin $\frac{1}{2}$ Pauli matrices (Appendix A).

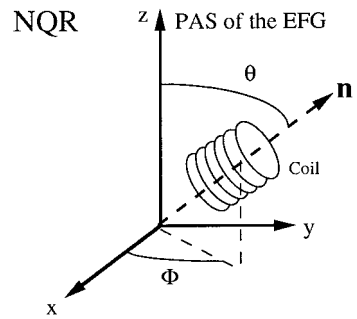

FIG. 1. Reference frames of an NQR experiment.

So, we obtained

$$Q = \frac{1}{3a} \{3\sigma_z \otimes \sigma_z + \eta\sqrt{3}\sigma_x \otimes I_2\}. \qquad [9]$$

When the sample is irradiated by a linearly polarized radiofrequency field (RF) of phase φ, the RF Hamiltonian H_{RF} is

$$H_{RF} = 2\omega_{RF}\cos(\omega t + \varphi)\mathbf{I}.\mathbf{n}, \qquad [10]$$

where $\omega_{RF} = \gamma B_1/2$, γ is the magnitude of the nuclear gyromagnetic ratio and ω the excitation angular frequency. Vectors are noted in bold letters. The coil axis is directed along the unity vector $\mathbf{n}$ whose coordinates are $\{\sin(\theta)\cos(\phi), \sin(\theta)\sin(\phi), \cos(\theta)\}$ in the PAS of the EFG (Fig. 1).

The time evolution of the spin-system under either $H = H_q$ for free evolution, or $H = H_q + H_{RF}$ during the pulses, is conveniently expressed by the density operator which obeys the von Neumann equation

$$\frac{d\rho}{dt} = i[\rho, H]. \qquad [11]$$

If the Hamiltonian were time independent, the formal solution of the Liouville equation would be

$$\rho(t) = e^{-iHt}\rho(0)e^{iHt}. \qquad [12]$$

However, this is rarely the case and approximations should be used (perturbation theory, average Hamiltonian theory (*1–3*)). When the Hamiltonian has one contribution which is much larger than the others, the approximations to describe the time evolution of the density operator are most conveniently described in the interaction representation where *all* the operators are transformed by the following unitary transformation

$$\tilde{A}(t) = UA(t)U^+, \qquad [13]$$

where $U = \exp(iTt)$ and U^+ is the hermitic conjugate of U. T is an hermitic operator.

Hence, applying this transformation to the density operator leads to

$$\frac{d\tilde{\rho}}{dt} = i[\tilde{\rho}, H_e] \quad \text{with } H_e = \tilde{H} - T. \tag{14}$$

The hermitic operator T may be chosen at will to simplify the resulting effective Hamiltonian.

Generally, when a small number of spins are involved, the most simple method to handle the evolution equation is to expand the density operator in a suitable complete set of orthogonal basis operators which span the operator space into which the density matrix evolves and to use the scalar product $\langle A/B\rangle = \mathrm{Tr}(AB)$, and the norm $\|A\|^2 = \mathrm{Tr}(A^2)$.

In NQR, the interaction representation is defined with respect to the pure quadrupolar Hamiltonian. For spins $I = \frac{3}{2}$, the property $Q^2 = I_4$ leads to formal simplifications and interesting relationships which are outlined in the following section.

II. INTERACTION REPRESENTATION WITH RESPECT TO AN OPERATOR SUCH THAT $Q^2 = I_4$

The interaction representation with respect to Q is defined by setting $U = e^{i\beta Q}$ in Eq. [13]. By expanding the exponential in a power series, the explicit expression of U can be easily obtained (see Table 1, cell 4). Consequently, the new operator $\tilde{A}$ becomes

$$\tilde{A} = e^{i\beta Q} A e^{-i\beta Q} = r_A + p_A \cos(2\beta) + q_A \sin(2\beta). \tag{15}$$

Thus, in the Q-interaction representation, an operator A is decomposed into three operators r_A, p_A, and q_A, which are defined in Table 1, cell 1. This table also summarizes the main properties of these operators. The first operator r_A is evidently the part which commutes with Q. The equations of cell 4 provides some solutions of the von Neumann equation, although a complete set of solutions could only be achieved by explicitly taking into account the peculiar nature of Q (see next section). Note the similarity of commutation relationships of cell 3 with the commutation relations of the Cartesian spin operators, except that the third expression does not make them cyclic unless $p_A q_A \sim Q$. Cell 2 indicates that as soon as the commutators or anticommutators of the type $[s_A, s_B]_\pm$ are known for one type of operator p or q, then they are known for the other one.

Since p_A and q_A have the same norm, it seems appropriate to define new operators s_{nA} ($s = p$ or q) such that

$$\mathrm{Tr}(s_{nA}^2) = \mathrm{Tr}(I_4) = 4 \tag{16}$$

$$s_{nA} = \sqrt{\frac{8}{\mathrm{Tr}(q_A^2)}}\, s_A = n_A s_A. \tag{17}$$

TABLE 1
Main Properties of the Operators r_A, p_A, q_A, Q

(1) Definition of the operators r_A, p_A, q_A:

$$Q^2 = I \text{ or } Q = Q^{-1}$$
$$r_A = \tfrac{1}{2}(A + QAQ)$$
$$p_A = \tfrac{1}{2}(A - QAQ)$$
$$q_A = \tfrac{i}{2}[Q, A]$$
$$p_A = iq_AQ = -iQq_A$$
$$\mathrm{Tr}(p_A^2) = \tfrac{1}{2}\{\mathrm{Tr}(A^2) - \mathrm{Tr}((AQ)^2)\}$$
$$\mathrm{Tr}(r_A p_A) = \mathrm{Tr}(r_A q_A) = 0$$

(2) Some relationships for operators related to different matrices $A \neq B$:

$$p_A p_B = q_A q_B$$
$$[p_A, p_B]_\pm = [q_A, q_B]_\pm$$
$$[q_B q_A, Q] = 0$$
$$[q_B, p_A] = iQ[q_A, q_B]_+$$
$$\text{if } [q_A, q_B]_+ = 0, \text{ then } [q_B, p_A] = 0$$

(3) Some commutators and anticommutators:

$$[p_A, Q] = 2iq_A$$
$$[Q, q_A] = 2ip_A$$
$$[p_A, q_A] = 2p_Aq_A = -2iQq_A^2$$
$$[p_A^2, Q] = [q_A^2, Q] = [p_Aq_A, Q] = 0$$
$$[s_A, Q]_+ = 0 \text{ for } s = p \text{ or } q$$
$$[p_A, q_A]_+ = 0$$

(4) Some trigonometric functions:

$$e^{i\beta Q} = \cos(\beta) + i\sin(\beta)Q$$
$$e^{i\beta Q} q_A e^{-i\beta Q} = q_A\cos(2\beta) - p_A\sin(2\beta)$$
$$e^{i\beta Q} p_A e^{-i\beta Q} = p_A\cos(2\beta) + q_A\sin(2\beta)$$

So, Eq. [15] can be rewritten as

$$\tilde{A} = r_A + n_A\{p_{nA}\cos(2\beta) + q_{nA}\sin(2\beta)\}. \tag{18}$$

III. APPLICATION TO THE PURE NQR OF SPIN $I = \frac{3}{2}$

Let us now apply the formalism developed in the preceding section to the problem of computing the NQR response to a multipulse sequence using the interaction representation with respect to operator Q.

Going into the interaction representation defined by choosing

$$T = \frac{\omega}{2} Q \tag{19}$$

and using

$$(\widetilde{\mathbf{I}.\mathbf{n}})(t) = r + \{p\cos(\omega t) + q\sin(\omega t)\} \tag{20}$$

gives the averaged or truncated Hamiltonian (zeroth order term in a Magnus expansion):

$$H = \frac{\Delta\omega}{2} \mathrm{Q} + \omega_{\mathrm{RF}}\{\cos(\varphi)p - \sin(\varphi)q\}. \qquad [21]$$

The first order correction in the Magnus expansion is smaller than the zeroth order term by approximately a factor of $\omega_{\mathrm{RF}}/\omega_q$. Thus, it is usually justified to neglect the correction terms of higher order than zero (for instance, $\nu_{\mathrm{RF}} < 100$ kHz and $\nu_q > 10$ MHz gives $\nu_{\mathrm{RF}}/\nu_q < 0.01$). Except for some factors, this Hamiltonian has the same structure as the NMR truncated Hamiltonian H_{RMN} in the rotating frame of a single spin subject to an off-resonance RF field of amplitude ω_1:

$$H_{\mathrm{NMR}} = \Delta\omega I_z + \omega_1\{\cos(\varphi)I_x + \sin(\varphi)I_y\}. \qquad [22]$$

To draw a complete analogy, we need the complete commutation relations of the operator set $\{Q, p, q\}$. In fact, only the commutator $[q, p]$ must be calculated.

The operators p and q of Eq. [21] are linear combinations of the $p_{n\alpha}$ or $q_{n\alpha}$ defined in Table 2

$$s = \sin(\theta)\cos(\phi)n_x s_{nx} + \sin(\theta)\sin(\phi)n_y s_{ny} + \cos(\theta)n_z s_{nz}, \qquad [23]$$

where $s = p$ or q and (θ, ϕ) are the polar angles of the coil axis in the PAS (Fig. 1).

Table 2 is a summary of some relations related to the operators s_α in a basis diagonalizing I_z. Appendix B indicates a fast method to compute the matrices defined by Pratt (*11*) as soon as their expression are known in a basis diagonalizing the quadrupolar Hamiltonian. We emphasize again that only a little algebra has to be performed in our formalism, since we only need to calculate the q_α because of the relations of Table 1. So, the cells 1, 3, and 4 of Table 2 are the most important. It may be remarked that only two parameters n_x and n_y are necessary to define the q_α and the p_α.

It is readily shown that the commutation relationships within a set $\{p_\alpha, q_\alpha, Q\}$ are cyclic up to a normalization factor. Combining these results with those of Table 1 leads to cell 4 where the case of a linear combination of the s_α is studied. The last commutator of cell 4 indicates that $[q, p]$ is indeed proportional to Q.

Thus, we are now able to define a new set of operators $\{Q_x, Q_y, Q_z\}$ by

$$Q_x = \frac{q}{2\lambda} \quad Q_y = \frac{p}{2\lambda} \quad Q_z = \frac{Q}{2}, \qquad [24]$$

where the angular factor $\lambda = \lambda(\theta, \phi)$ is a function of the polar angles which specify the orientation of the coil with respect to the PAS of the EFG. It is given by

TABLE 2
***Q* Interaction Representation of the Spin Operators in a Basis Diagonilizing I_z**

(1) Operators $q_{I\alpha} = q_\alpha$:

$$q_x = n_x q_{nx} = -n_x\sigma_z \otimes \sigma_y \text{ with } n_x = \frac{3+\eta}{2a\sqrt{3}}$$
$$q_y = n_y q_{ny} = n_y\sigma_z \otimes \sigma_x \text{ with } n_y = \frac{3-\eta}{2a\sqrt{3}}$$
$$q_z = n_z q_{nz} = n_z\sigma_y \otimes I_2 \text{ with } n_z = \frac{\eta}{a\sqrt{3}}$$

Note that the n_α are not independent since $n_z = n_x - n_y$

(2) Operators $p_{I\alpha} = p_\alpha$:

$$p_x = n_x p_{nx} = \frac{n_x}{3a}\{3I_2 \otimes \sigma_x + \eta\sqrt{3}\,\sigma_y \otimes \sigma_y\}$$
$$p_y = n_y p_{ny} = \frac{n_y}{3a}\{3I_2 \otimes \sigma_y - \eta\sqrt{3}\,\sigma_y \otimes \sigma_x\}$$
$$p_z = n_z p_{nz} = \frac{n_z}{3a}\{-3\sigma_x \otimes \sigma_z + \eta\sqrt{3}\,\sigma_z \otimes I_2\}$$

(3) Main properties:

$$(q_\alpha)^2 = (n_\alpha)^2 I_4 = (p_\alpha)^2$$
$$p_\alpha q_\alpha = -i(n_\alpha)^2 Q$$
$$[q_\alpha, q_\beta]_+ = [p_\alpha, p_\beta]_+ = 0 \text{ if } \alpha \neq \beta$$
$$[q_\alpha, p_\beta] = 0 \text{ if } \alpha \neq \beta$$
$$[p_\alpha, Q] = 2iq_\alpha$$
$$[Q, q_\alpha] = 2ip_\alpha$$
$$[q_\alpha, p_\alpha] = 2i(n_\alpha)^2 Q$$

(4) If $A = \Sigma_\alpha a_\alpha I_\alpha$

$$s_A = \Sigma_\alpha a_\alpha s_\alpha \text{ for } s = p \text{ or } q$$
$$s_A^2 = \Sigma_\alpha (a_\alpha n_\alpha)^2 I_4$$
$$[q_A, p_A] = 2i\Sigma_\alpha (a_\alpha n_\alpha)^2 Q$$

$$\lambda(\theta, \phi) = \frac{1}{2a\sqrt{3}} \times \sqrt{4\eta^2\cos^2(\theta) + \sin^2(\theta)[9 + \eta^2 + 6\eta\cos(2\phi)]}. \qquad [25]$$

This angular factor is the norm of p and q.

These normalized operators $Q_\alpha(\mathrm{Tr}[(Q_\alpha)^2] = 1)$ fulfill the same commutation relations as the Cartesian spin operators

$$[Q_x, Q_y] = iQ_z \text{ and cyclic permutations.} \qquad [26]$$

As a consequence, they are also orthogonal with respect to the trace

$$\mathrm{Tr}[Q_\alpha Q_\beta] = \delta_{\alpha\beta} \quad \text{for } \alpha = x, y, z. \qquad [27]$$

We stress again that the Q_α are defined for one orientation of

TABLE 3

Evolution of the Set of Operators $\{O_+, O_z, O_-\}$ under the Time-Independent Hamiltonian: $H_p = \Delta\omega O_z + \omega_1 \{\cos(\varphi) O_x + \sin(\varphi) O_y\}$, where $O_\pm = O_x \pm iO_y$ and the O_α Fulfil the Commutation Relations $[O_x, O_y] = iO_z$ and the Other Cyclic Permutations, $H_L = \Delta\omega O_z$ is the Free Evolution Hamiltonian

A	Evolution under a RF pulse of length t $e^{iH_p t}Ae^{iH_p t}$	Free evolution $e^{iH_p t}Ae^{iH_L t}$
O_+	O_+ $\frac{1}{2}\{2\cos(v) + \cos^2(u)[1 - \cos(v)] - 2i\sin(v)\sin(u)\}$ O_z $\cos(u)\{\sin(u)[1 - \cos(v)] + i\sin(v)\}e^{i\varphi}$ O_- $\frac{1}{2}\cos^2(u)[1 - \cos(v)]e^{i2\varphi}$	$O_+ e^{-i\Delta\omega t}$
O_z	O_+ $\frac{1}{2}\cos(u)\{\sin(u)[1 - \cos(v)] + i\sin(v)\}e^{-i\varphi}$ O_z $\cos^2(u)\cos(v) + \sin^2(u)$ O_- $\frac{1}{2}\cos(u)\{\sin(u)[1 - \cos(v)] - i\sin(v)\}e^{i\varphi}$	O_z
O_-	O_+ $\frac{1}{2}\cos^2(u)[1 - \cos(v)]e^{-i2\varphi}$ O_z $\cos(u)\{\sin(u)[1 - \cos(v)] - i\sin(v)\}e^{-i\varphi}$ O_- $\frac{1}{2}\{2\cos(v) + \cos^2(u)[1 - \cos(v)] + 2i\sin(v)\sin(u)\}$	$O_- e^{i\Delta\omega t}$

Where

$v = \omega_e t$ is the effective nutation angle

$\omega_e = \sqrt{\Delta\omega^2 + \omega_1^2}$

$\cos(u) = \dfrac{\omega_1}{\omega_e}$ and $\sin(u) = \dfrac{\Delta\omega}{\omega_e}$

the PAS with respect to the coil. Expressed on this basis, the secular part of the NQR Hamiltonian during a pulse reads

$$H = \Delta\omega Q_z + \lambda'\omega_{RF}\{\cos(\zeta)Q_x + \sin(\zeta)Q_y\}, \qquad [28]$$

where we have shifted the pulse phase as $\zeta = \pi/2 + \varphi$ to obtain the same Hamiltonian as H_{NMR}. This is possible because only the relative phases between the pulses are relevant to the calculations. We also defined a reduced angular factor as $\lambda' = 2\lambda$.

The signal detected in the coil with a quadrature detection setup is proportional to the lowpass filtered (LP) signal (or time averaged signal over one period of the RF field)

$$s(t) \sim \mathrm{LP}[\mathrm{Tr}\{\mathbf{I}.\mathbf{n}e^{-i\omega t}\rho(t)\}] = \mathrm{LP}[\mathrm{Tr}\{(\widetilde{\mathbf{I}.\mathbf{n}})(t)e^{-i\omega t}\tilde{\rho}(t)\}]. \qquad [29]$$

Noting that Eq. [20] could be rewritten as

$$(\widetilde{\mathbf{I}.\mathbf{n}})(t) = r - \lambda i\{Q_+ e^{i\omega t} - Q_- e^{-i\omega t}\} \qquad [30]$$

and that $\mathrm{Tr}(pr) = \mathrm{Tr}(qr) = 0$ results in (we disregarded some irrelevant factors)

$$s(t) \sim \lambda'\mathrm{Tr}\{(Q_x + iQ_y)\tilde{\rho}(t)\} = \lambda'\mathrm{Tr}\{Q_+\tilde{\rho}(t)\}. \qquad [31]$$

In the high temperature approximation, the equilibrium Boltzmann density matrix is proportional to Q: $\rho_{eq} \sim Q$, so the initial condition is taken as

$$\tilde{\rho}(0) = \rho(0) = Q_z. \qquad [32]$$

Hence, it is readily seen from the above considerations that the formalism describing the time evolution of the pure NQR of a spin $I = \frac{3}{2}$ is completely analogous to the high field NMR of a single isolated spin irradiated off-resonance, whose truncated Hamiltonian in the rotating frame is H_{NMR} (Eq. [22]). It means that under the Hamiltonian of Eq. [28], the density matrix evolves only within a linear combination of the three operators $\{Q_+, Q_z, Q_-\}$. Therefore, the corresponding notions of coherence transfer pathways of ± 1 quantum and zero quantum could be used, as well as the vector model for the set $\{Q_x, Q_y, Q_z\}$. Moreover, the phase cycling of NQR multipulse sequences can be derived from the same rules as in NMR, using the selection of coherence pathways, limited here only to the three values $\{-1\ 0\ 1\}$.

In practice, the same formula as calculated in NMR could be used by replacing NMR's ω_1 by $\lambda'\omega_{RF}$ and multiplying the resulting expression by λ'. The basic formula for the time evolution of a general set $\{O_+, O_z, O_-\}$ are recalled in Table 3.

The calculation scheme would be the following:

—The contribution of a single coherence pathway is given by the product of the factors of Table 3 corresponding to the coherence jumps or to the free evolution periods.

—The resulting signal is the sum of all the contributions of the coherence pathways selected by the phase cycling proce-

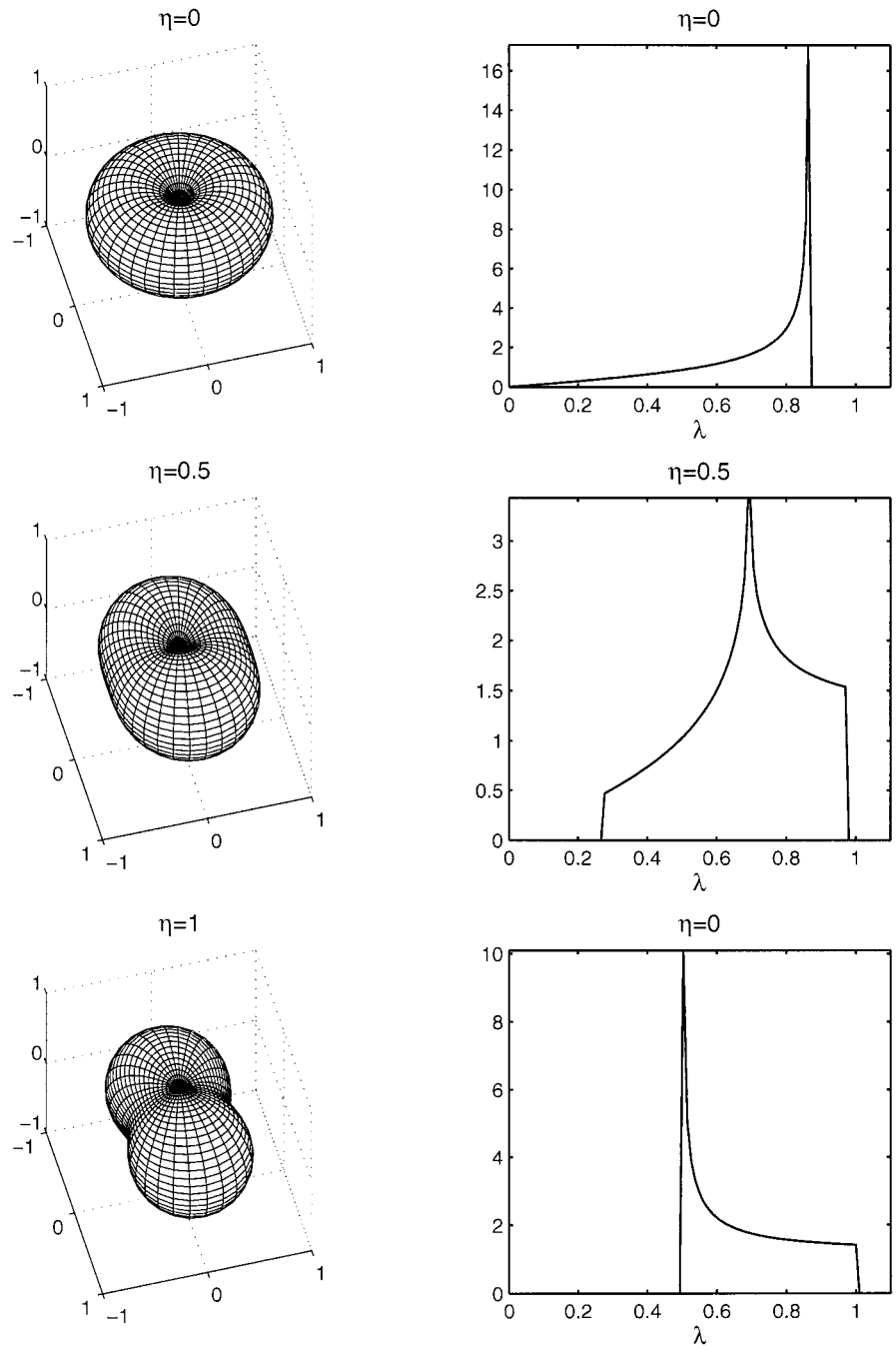

FIG. 2. Angular factor $\lambda(\theta, \phi)$ for different values of the asymmetry parameter. The left side of the figure shows the angular dependence of λ (the surface is the locus of a segment of length λ for all angles (θ, ϕ)) whereas the right side is a plot of the probability of having a given value of λ (all curves are normalized).

dure, which arrive at the coherence level -1 (it is the factor of Q_- in the expansion of the density matrix on the basis $\{Q_+, Q_z, Q_-\}$).

In the case of a powder sample, an average over all the equally probable relative orientations of the solenoid coil axis with respect to the PAS of the EFG should be performed, and it is the object of the next section.

IV. POWDER AVERAGE OF THE EXCITATION AND DETECTION

In contrast to NMR where the frequency is modulated by the crystallite orientation, the particularity of pure NQR is that only one frequency is observed if the powder sample has only one quadrupolar site. Therefore, the spectrum width is solely a

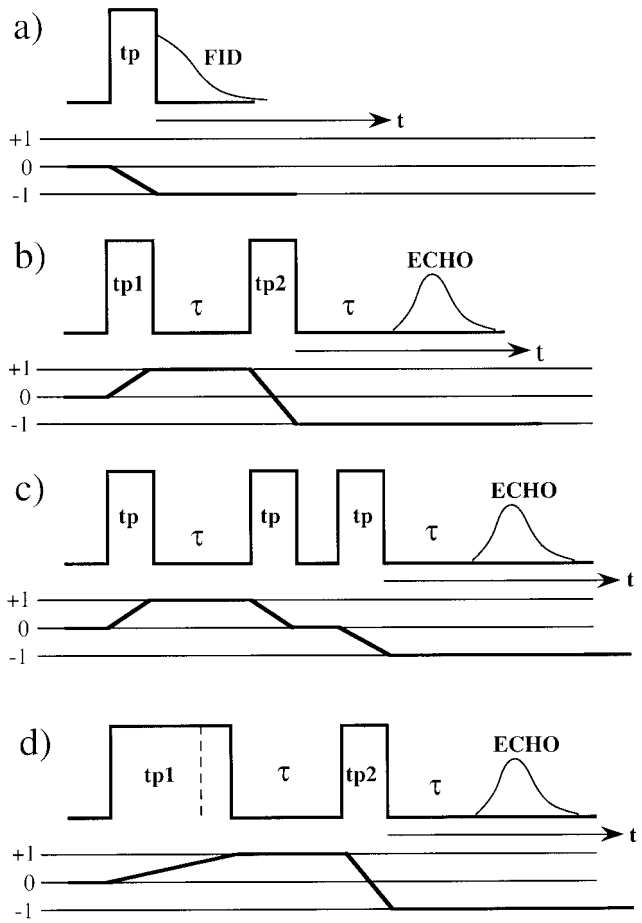

FIG. 3. Pulse sequences and their coherence pathways. (a) A single pulse sequence $\{\theta\}$; (b) two-pulse sequence $\{\theta_1\}$ $\{\theta_2\}$ giving an echo. $\{\theta\}$ $\{2\theta\}$ is the Hahn sequence; (c) Three-pulse sequence of same length $\{\theta\}$ $\{\theta\}$ $\{\theta\}$ giving an echo. The coherence pathway $0 \rightarrow +1 \rightarrow 0 \rightarrow -1$ is chosen by appropriate cycling of pulse phases using the general NMR rules ("stimulated echo" sequence). The delay between the first and second pulse will determine the echo, whereas the delay between the second and third pulse has no real influence since the zero-quantum pathway is selected (It must be much smaller than the relaxation time T_1). (d) Nutation experiment with one or two pulses. The signal is Fourier-transformed with respect to the first pulse length to obtain the nutation spectrum. One can also use a second pulse of fixed angle to obtain an echo.

consequence of a distribution of EFG values and of dipolar interactions, simplifying the interpretation of the spectrum. In fact, the angular factor $\lambda(\theta, \phi)$ affects both the excitation and the reception, respectively, through the $\lambda(\theta, \varphi)\omega_{RF}$ term which modulates the nutation frequencies of the isochromats and through the signal amplitude factor $\lambda(\theta, \varphi)$ which renders the amplitude of the signal angular dependent. In some ways, this situation is analogous to the modulation of the nutation frequencies in NMR by inhomogeneities in the RF field produced by an irregular solenoid coil.

In powder samples, all angles (θ, ϕ) are distributed randomly. The powder average is usually calculated by performing an average other all crystallites orientations. But this method is rather time consuming because about 10^5 different orientations are usually needed to sample the whole space. A much more efficient method is to perform the average over the values of λ, using the probability density $g(\lambda)$ of values of λ. This probability density can be calculated analytically by using the results of Appendix I of Slichter (*2*). As a matter of fact, we noted that

$$\lambda(\theta, \phi) = \frac{1}{A}\sqrt{R(z, \phi)}, \qquad [33]$$

where

$$A = 2\sqrt{3 + \eta^2} \qquad [34]$$

$$z = -\cos(\theta) \qquad [35]$$

$$R(z, \phi) = (3 + \eta)^2 - 12\eta \sin^2(\phi) + z^2[4\eta^2 - (3 + \eta)^2 + 12\eta \sin^2(\phi)]. \qquad [36]$$

The probability density of values of R being known, we deduce the probability density $g(\lambda)$ as

$$g(\lambda) = \frac{2A^2}{|b|}\lambda D\left[\frac{(A\lambda)^2 - c}{b}, f\right] \qquad [37]$$

with

$$f = \frac{-12\eta}{b};\ c = (3 + \eta)^2;\ b = 3(\eta - 3)(\eta + 1) \qquad [38]$$

and the function $D(y, f)$ is defined by

$$D(y, f) = \begin{cases} y < f & \dfrac{1}{\pi\sqrt{f(1-y)}} K\left[\dfrac{y(1-f)}{(1-y)f}\right] \\ y > f & \dfrac{1}{\pi\sqrt{y(1-f)}} K\left[\dfrac{f(1-y)}{(1-f)y}\right] \end{cases}, \qquad [39]$$

where K is the complete elliptic integral of the first kind (*18*).

The angular variation of λ is visualized on Fig. 2 as well as the probability density $g(\lambda)$ for three values of η. At $\eta = 0$, there is no excitation when the coil lies along the z axis of the PAS. The angular character is exactly the same as the spherical harmonic $Y_{1\pm1}$. As η increases, the excitation along z increases, whereas it becomes less efficient along y, the excitation profile being distorted from azimuthal symmetry.

The minimum and maximum values of λ are, respectively,

$$\lambda_{min} = \frac{\eta}{a\sqrt{3}} \quad \text{(coil along the } z \text{ axis)} \qquad [40]$$

$$\lambda_{max} = \frac{3}{2}\frac{1 + \dfrac{\eta}{3}}{a\sqrt{3}} \quad \text{(coil along the } x \text{ axis)}. \qquad [41]$$

TABLE 4
Explicit Expressions for the Signal Detected after the One- to Three-Pulse Sequences of Figs. 3a–3c

One pulse of phase φ (Fig. 3a): $(\theta)_{\varphi} - t$

$$S_p(\theta, \Delta x, t) = \{S_{pr} + iS_{pi}\}e^{i\varphi}e^{i\Delta\omega t} \quad \text{with}$$
$$S_{\text{pr}} = \frac{(\lambda')^2}{2}\frac{\Delta x}{(\omega_N)^2}[1 - \cos(\theta\omega_N)]$$
$$S_{pi} = -\frac{(\lambda')^2}{2}\frac{1}{(\omega_N)}[\sin(\theta\omega_N)]$$

Two pulses (Fig. 3b): $(\theta_1)_{\varphi 1} - \tau - (\theta_2)_{\varphi 2} - t$

$$S_{pp}(\theta_1, \theta_2, \tau, \Delta x, t) = \{S_{ppr} + iS_{ppi}\}\exp[i(2\varphi_2 - \varphi_1)]\exp[i\Delta\omega(t - \tau)] \quad \text{with}$$
$$S_{ppr} = \frac{(\lambda')^4}{4}\frac{\Delta x}{(\omega_N)^4}[1 - \cos(\theta_1\omega_N)][1 - \cos(\theta_2\omega_N)]$$
$$S_{ppi} = -\frac{(\lambda')^4}{4}\frac{1}{(\omega_N)^3}[\sin(\theta_1\omega_N)][1 - \cos(\theta_2\omega_N)]$$

Three pulses (Fig. 3c): $(\theta)_{\varphi 1} - \tau - (\theta)_{\varphi 2} - (\theta)_{\varphi 3} - t$

$$S_{ppp}(\theta, \tau, \Delta x, t) = \frac{(\lambda')^4}{4}\frac{1}{(\omega_N)^3}K^2K^*\exp[i(\varphi_2 + \varphi_3 - \varphi_1)]\exp[i\Delta\omega(t - \tau)]$$
$$\text{with } K = \left\{\frac{\Delta x}{\omega_N}[1 - \cos(\theta\omega_N)] - i\sin(\theta\omega_N)\right\}.$$

Where

$\Delta x = \dfrac{\Delta\omega}{\omega_{\text{RF}}}$ is the dimensionless frequency offset

$\omega_N = \sqrt{\Delta x^2 + (\lambda')^2}$ and $\theta_i = \omega_{\text{RF}}t_i$ the flip angle of pulse number i.

$\lambda' = 2\lambda(\theta,\phi)$ is defined in the text, Eq. [25].

Note. For a powder sample, an average over the range of values of λ' should be performed as explained in the text.

The divergence of the probability density $g(\lambda)$ or of the nutation spectrum comes from the contribution of crystallites whose y axis lie along the coil, and occurs at

$$\lambda_{\text{div}} = \frac{3}{2}\frac{1 - \dfrac{\eta}{3}}{a\sqrt{3}} \quad (\text{coil along the } y \text{ axis}). \qquad [42]$$

The powder average of signal $S(t, \lambda)$ is then

$$\langle S(t, \lambda)\rangle = \int_{\lambda_{\min}}^{\lambda_{\max}} g(\lambda)S(t, \lambda)d\lambda. \qquad [43]$$

The angle brackets indicate an average over the probability density $g(\lambda)$.

Note that the mean value $\langle\lambda\rangle \approx 0.686$ and second moment $\langle\lambda^2\rangle \approx 0.5$, as obtained by numerical integration, are almost independent of the asymmetry parameter. Thus, these quantities cannot be used to get information on the asymmetry parameter.

So, the problem of computing a powder average reduces to the numerical integration of Eq. [43]. We found that it is enough to sample the range of λ values over 100 points in order to get accuracy, instead of performing a double integration over more than 10^4 points in the conventional method.

V. THEORETICAL AND EXPERIMENTAL STUDY OF ONE- TO THREE-PULSE SEQUENCES FOR POWDER SAMPLES

It is not obvious at first sight whether the strategies developed in NMR to optimize pulse sequences are also valid in the pure NQR of a powder sample because of the angular average over both the excitation and the reception. Therefore, in order to illustrate the methods developed in the last two sections, we will draw a comparison of the relative efficiencies of the sequences depicted on Fig. 3 by considering briefly the effect of the pulse length and off-resonance irradiation on the signal amplitude, the excitation bandwidth, and phase linearity. We will also study the shape of the nutation spectra obtained with the sequences of Fig. 3d. The simulations are compared to

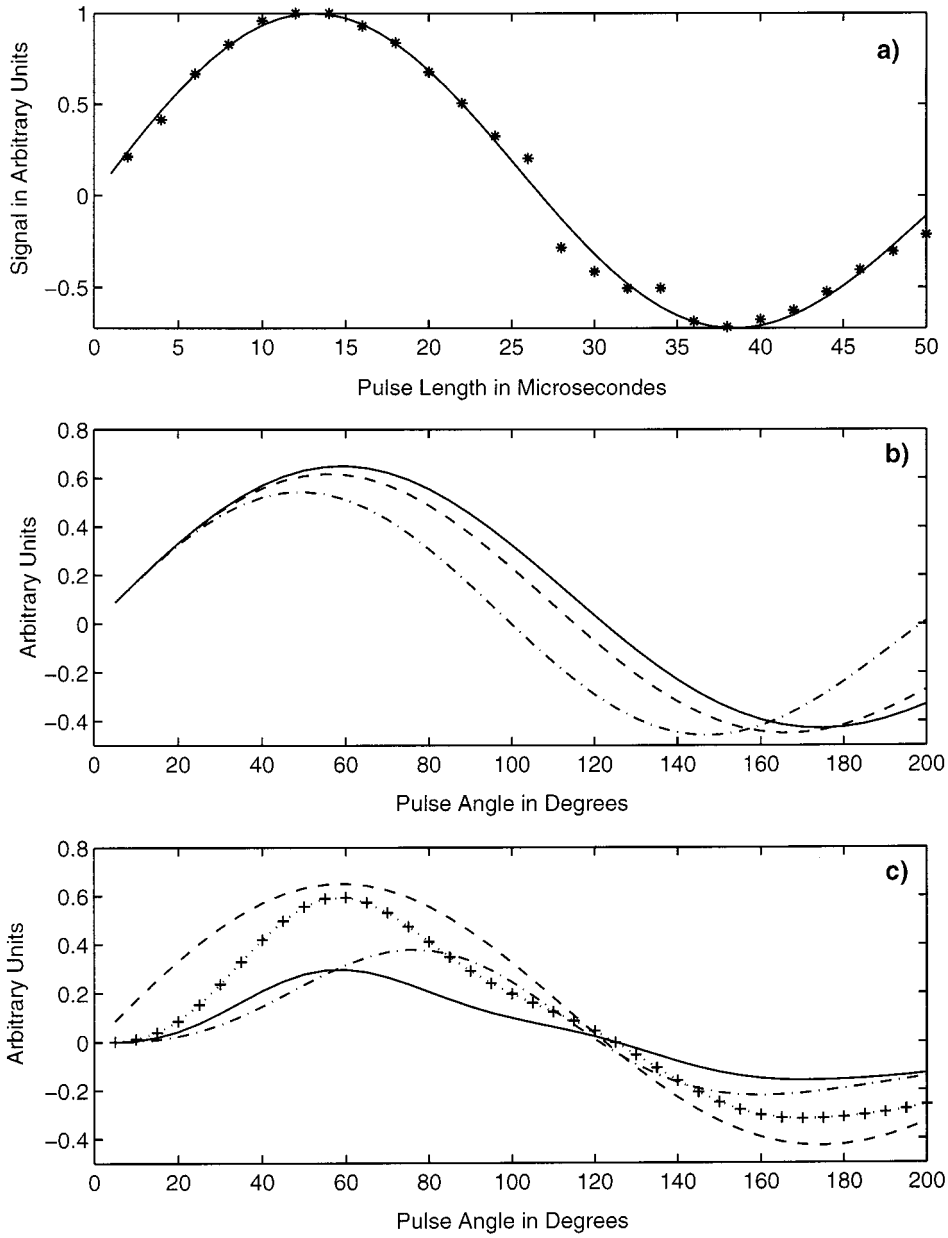

FIG. 4. (a) Experimental and simulated maximum of the spectrum of the high frequency line of Chloranil obtained with a single pulse of varying length applied on resonance. The stars (*) are the experimental values and the continuous line is the best fit obtained from Eq. [44] ($\eta \approx 0.2$). The resulting radio frequency power is $\nu_{RF} \approx 12.5$ kHz. (b) Simulated signal amplitude of $\{\theta\}$ for different pulse angles and reduced frequency offset $\Delta x = \Delta\omega/\omega_{RF}$. On resonance, solid line; off resonance, dashed line $\Delta x = 0.5$ and dash–dot line $\Delta x = 1$. (c) Effect of the pulse angle for the four sequences studied in the text, with irradiation on-resonance ($\eta = 0.5$; pulse angle $\theta = \omega_{RF}\, t_p$). Dashed line, single pulse $\{\theta\}$; Dash–dot line, two-pulse echo sequence $\{\theta\}\ \{\theta\}$; Continuous line, three-pulse stimulated echo sequence $\{\theta\}\ \{\theta\}\ \{\theta\}$; Dotted line and +, Hahn-echo sequence $\{\theta\}\ \{2\theta\}$.

experimental results obtained with Chloranil at ambient temperature.

^{35}Cl is a typical spin $I = \frac{3}{2}$ nucleus, with a Zeeman splitting of ~30 MHz in a ~7 T field and quadrupolar energies of covalently bound Cl being roughly in the interval ~30–40 MHz. As a model compound, we choose powder Chloranil (Aldrich), because its line width is sufficiently small to be detected by a single pulse and it gives a good signal at large frequency offsets. It was used without purification. Chloranil has two ^{35}Cl lines around 36.855 and 36.785 MHz, depending on temperature, with asymmetry parameter $\eta \approx 0.2$ almost equal for the two lines (see however (*13*)). The line width at half height is a few kHz, and is inhomogeneous because a hole can be burnt into the line with a long saturating pulse.

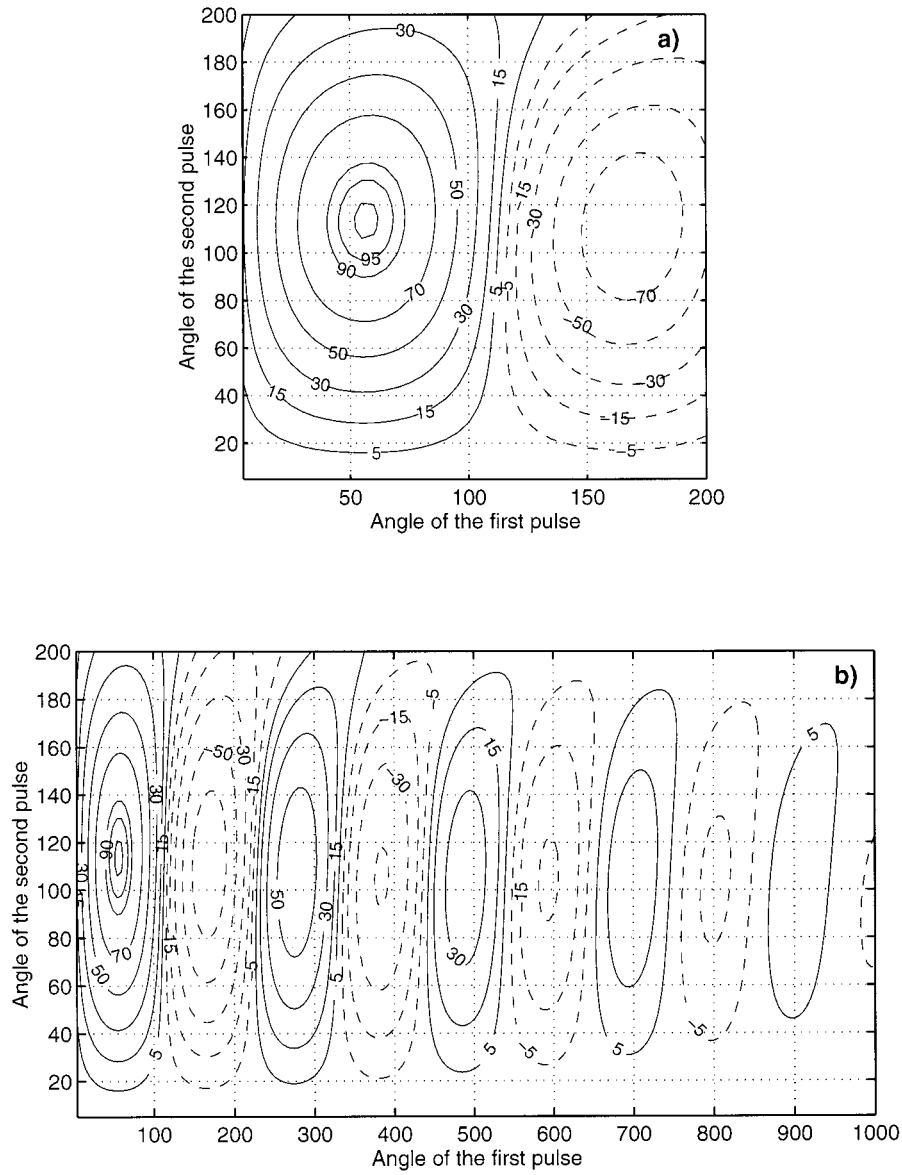

FIG. 5. Constant echo amplitude lines of a two-pulse echo sequence $\{\theta_1\}\ \{\theta_2\}$ with respect to their effective angles $\theta_i = \omega_{RF}\, t_{pi}$. Irradiation is assumed on resonance, and $\eta = 0.2$. (a) The set of dashed isoclines corresponds to a negative signal. (b) The range of values of θ_1 is extended to cover nutation experiments using an echo to detect the signal (Fig. 3d).

All experiments were performed on a Bruker ASX 300 at ambient temperature, with the static Bruker probe lying at least 5 m away from the ~7 T magnet (we checked that the residual static field at this distance was comparable to the Earth's magnetic field with a Gauss meter. Experimentally, the distortion of the spectrum by the splitting of the pure NQR energy level is small enough to be undetectable). All spectra were acquired with quadrature detection. The probe full bandwidth at half height was roughly ~400 kHz. The delay between the two last pulses of sequence $\{\theta\}\ \{\theta\}\ \{\theta\}$ was arbitrarily set to 20 μs (a time much smaller than T_1, and about twice as long as the dead time).

The complete expressions of the outcomes of sequences of Figs. 3a–3c, with respect to time counted from the end of the last pulse, the dimensionless frequency offset and the pulse angles can be found in Table 4. The expressions of Table 4 were obtained by means of the calculation scheme proposed in Section III, and are in agreement with references (*11*) and (*16*) for single and two pulse sequences, and with reference (*5*) for the three-pulse sequence, although our result is more general in

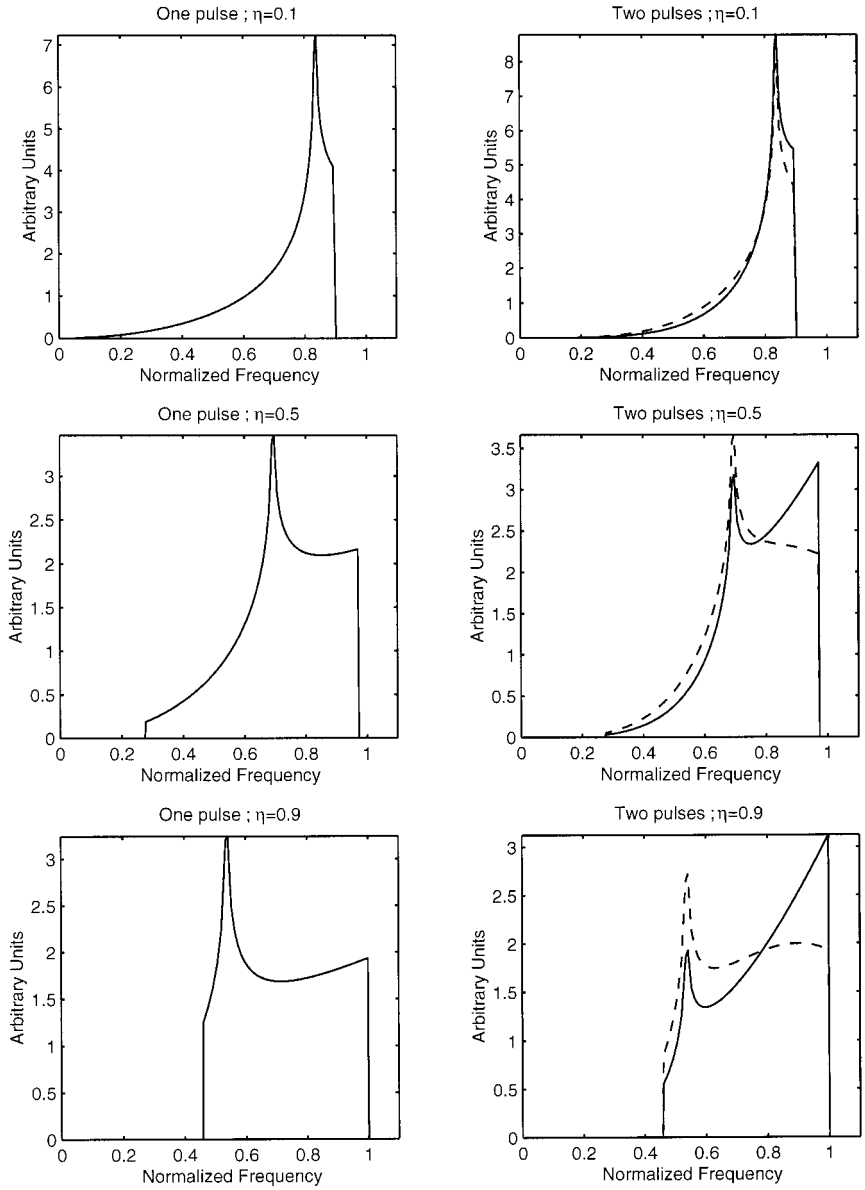

FIG. 6. Simulated nutation spectra for different values of the asymmetry parameter. On the left side are sketched the single pulse nutation experiments. On the right side, a second pulse of length θ_2 is added to get an echo: solid line, $\theta_2 = \theta_M$; dashed line, $\theta_2 = 2\theta_M$. All spectra are normalized, $\eta = 0.5$.

the last case. The powder average, although performed for the simulations, is not indicated to clarify notations.

On resonance, the signal amplitude simplified as

$$S_p(\theta) = \frac{\lambda'}{2}\sin(\lambda'\theta) \qquad [44]$$

$$S_{pp}(\theta_1, \theta_2) = \frac{\lambda'}{4}[\sin(\lambda'\theta_1)][1 - \cos(\lambda'\theta_2)] \qquad [45]$$

$$S_{ppp}(\theta) = \frac{\lambda'}{4}\sin^3(\lambda'\theta), \qquad [46]$$

where all phase factors have been set to unity and $\theta = \omega_{RF}t_p$ is the pulse "nutation angle." These amplitudes are all proportional to λ'. The NMR case corresponds to $\lambda' = 1$.

The first point we deal with is the optimization of the pulse length to give the maximum signal. For on-resonance irradiation, the signal amplitude of a single pulse sequence is modulated by a sine function of the pulse length t_p in both NMR and NQR (Eq. [44]). Hence, the maximum occurs when the effective total pulse angle is such that $\lambda'\theta = \pi/2$. In NQR, this condition can only be rigorously achieved for a given crystallite or a monocrystal. For a polycrystalline sample, the resulting function is no more a sine function of the pulse length (Fig.

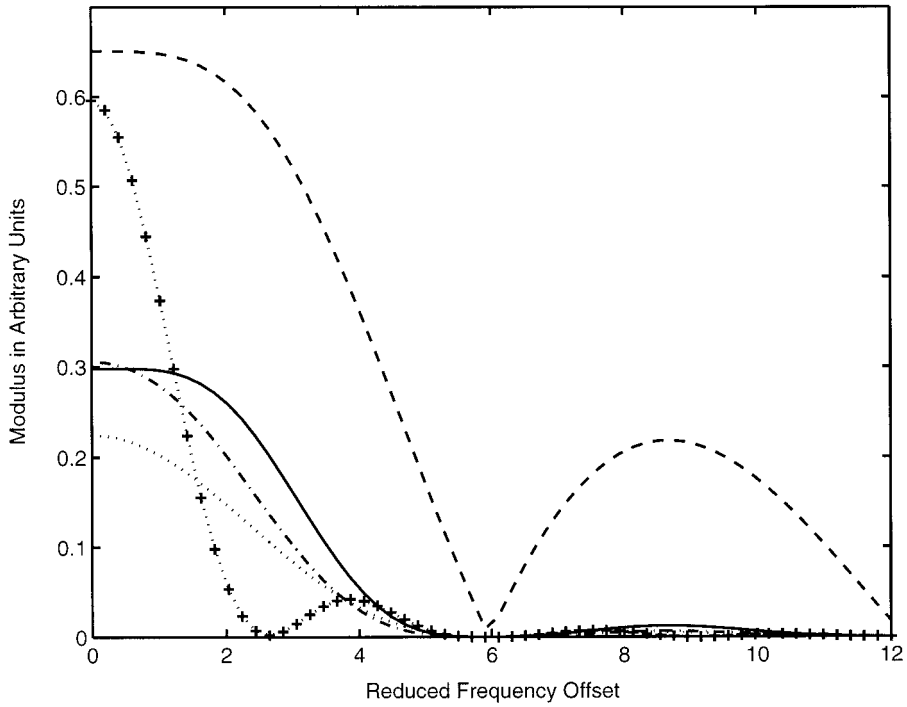

FIG. 7. Simulated excitation bandwidth of the four sequences studied in the text ($\eta = 0.2$). The reduced frequency offset is $\Delta x = \Delta\omega/\omega_{RF}$. Dashed line, $\{\theta_M\}$; dash–dot line, $\{\theta_M\}$ $\{\theta_M\}$; continuous line, $\{\theta_M\}$ $\{\theta_M\}$ $\{\theta_M\}$; dotted line with +, $\{\theta_M\}$ $\{2\theta_M\}$; dotted line, $\{\theta_M/2\}$ $\{\theta_M\}$.

4a). The maximum signal is observed at pulse angle θ_M defined by

$$\theta_M \approx \frac{1.1}{\sqrt{3}}\frac{\pi}{2} \approx 0.64\,\frac{\pi}{2}. \qquad [47]$$

This value is smaller than $\pi/2$ because the scaling factors λ' render the nutation of isochromats more efficient on average than in the case of NMR; indeed, $\lambda' = 1$ for NMR whereas $\langle\lambda'\rangle \approx 1.4$ for NQR. As illustrated by Fig. 4a, the comparison of the experiments and the simulation is rather good. The value of the radio frequency power as defined by Eq. [28] was obtained with a least square fitting procedure and gave $\nu_{RF} \approx 12.5$ kHz.

Irradiating off-resonance decreases slightly the pulse angle at which the maximum signal occurs, as well as signal intensity, but the effect is rather small even for resonance offsets of $\Delta x \approx 0.5$.

Figure 4c compares the outcomes of pulse sequences of Figs. 3a–3c for different pulse angles with irradiation on-resonance. The maximum signal is observed at almost the same pulse angle θ_M for sequences $\{\theta\}$, $\{\theta\}$ $\{2\theta\}$, and $\{\theta\}$ $\{\theta\}$ $\{\theta\}$, whereas it is shifted to higher values for the $\{\theta\}$ $\{\theta\}$ sequence, as in NMR. The signal vanishes for all sequences at the same angle. Unlike the case of NMR, the maximum signal of the $\{\theta\}$ $\{2\theta\}$ sequence is slightly less than the one of the $\{\theta\}$ sequence, because all the isochromats are not refocused exactly. For pulse angles smaller than θ_M, the sequence $\{\theta\}$ $\{\theta\}$ $\{\theta\}$ is more efficient than the sequence $\{\theta\}$ $\{\theta\}$.

To get further insight in the behavior of the echo sequence $\{\theta_1\}$ $\{\theta_2\}$, we also plotted the lines of constant echo magnitude in Fig. 5a. The curves are elongated quasi-ellipses along the θ_2 axis, centered around $\theta_1 = \theta_M \approx 57.5°$ and $\theta_2 \approx 115°$, the ratio θ_2/θ_1 being roughly 2, like in NMR. The line at 95% of maximum signal indicates that the maximum is rather broad, showing that a large range of angle values gives a good signal.

In the experiments described below, the pulse angle was the main variable, as in nutation experiments (Fig. 3d). In fact, the experiment to optimize the signal amplitude is a nutation experiment stopped at short pulse lengths. The nutation spectrum is obtained by the sine-Fourier-transform of the signal amplitude with respect to the first pulse length.

The problem of choosing the second pulse angle arises. The experimenter would certainly intuitively choose $\theta_2 \approx 2\theta_M$, which corresponds to the optimized effective "π pulse" for the Hahn-echo sequence $\{\theta_M\}$ $\{2\theta_M\}$. As shown by Fig. 5b, which is an extended version in the θ_1 direction of Fig. 5a, this choice seems to be good because the horizontal line drawn from $\theta_2 \approx 2\theta_M$ almost cross all the centers of the ellipses. We will show below that this choice also minimizes the distortion of the spectrum as compared to a single pulse nutation spectrum. Note that the signal decreases below 10% of the maximum signal when $\theta_1 \geq 900°$, indicating that longer nutation pulses are useless (provided that arcing or heating have not stopped the experiment before that value).

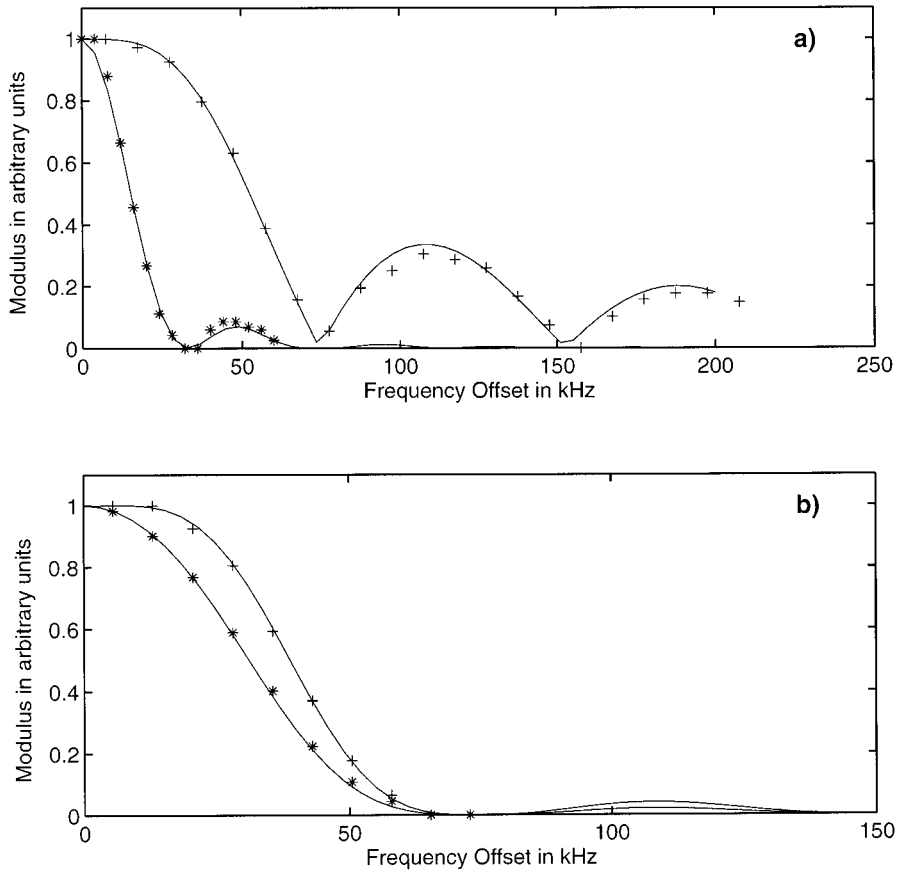

FIG. 8. Experimental and simulated excitation/reception bandwidth of different pulse sequences. (a) (+) Single pulse of 13 μs; (*) Hahn sequence $\{\theta\}\ \{2\theta\}$ with $\theta \sim 13$ μs. (b) (*) two-pulse echo sequence $\{\theta\}\ \{\theta\}$; (+) Three-pulse sequence $\{\theta\}\ \{\theta\}\ \{\theta\}$ with coherence pathway 0 +1 0 −1. All pulses have the same length (13 μs). The solid lines are the theoretical results with $\nu_{RF} \approx 12.5$ kHz, $\eta = 0.2$. All the amplitudes are normalized to one.

The results of Section IV allow us to determine the analytical expression of the nutation spectrum. If we let $x = \nu/2\nu_{RF}$, then the spectra are proportional to

$$F_{nut1}(x) \sim xg(x) \quad [48]$$

$$F_{nut2}(x) \sim xg(x)[1 - \cos(2\theta_2 x)], \quad [49]$$

where the probability density $g(x)$ is given by Eq. [37]. The first expression corresponds to a single pulse excitation, whereas the second expression comes from a two-pulse nutation sequence with a second pulse of flip-angle $\theta_2 = \omega_{RF} t_{p2}$. Such spectra appear in Fig. 6. It turns out that the shapes of the spectra obtained from the two sequences are very similar for a given asymmetry parameter when $\theta_2 \approx 2\theta_M$. As remarked by Harbison (*13*), the singularities are obviously at the same values of x for both sequences. The proposed analytical expressions can be useful to perform a least-square fitting of the experimental spectra. This approach could be extended to the case of off-resonance spectra.

So far, we have mainly considered that the irradiation was performed exactly on-resonance. But off-resonance effects cannot be neglected in real experiments where the width of the spectrum may be rather large (>100 kHz). The acquisition of broad spectra is then limited by the excitation bandwidth of the pulse sequence because the highest available RF powers are not infinite (currently, the RF powers are a few tens of kHz). The main effect that can be observed is a deformation in the shape of the spectrum, which becomes only severe when the RF power is less than or of the order of magnitude of the spectrum full width. In general, a large excitation bandwidth can only be achieved at the expense of either a reduction of the signal to noise ratio or an increase of the experiment duration. Hence, a compromise should be found. For very broad lines, a reconstruction scheme has been proposed (*16*) to retrieve the full spectrum by adding truncated subspectra acquired from a regularly spaced set of irradiation frequencies which covers the whole spectrum width.

Nevertheless, some situations require a uniform excitation over the entire spectrum. A rapid inspection of the expressions

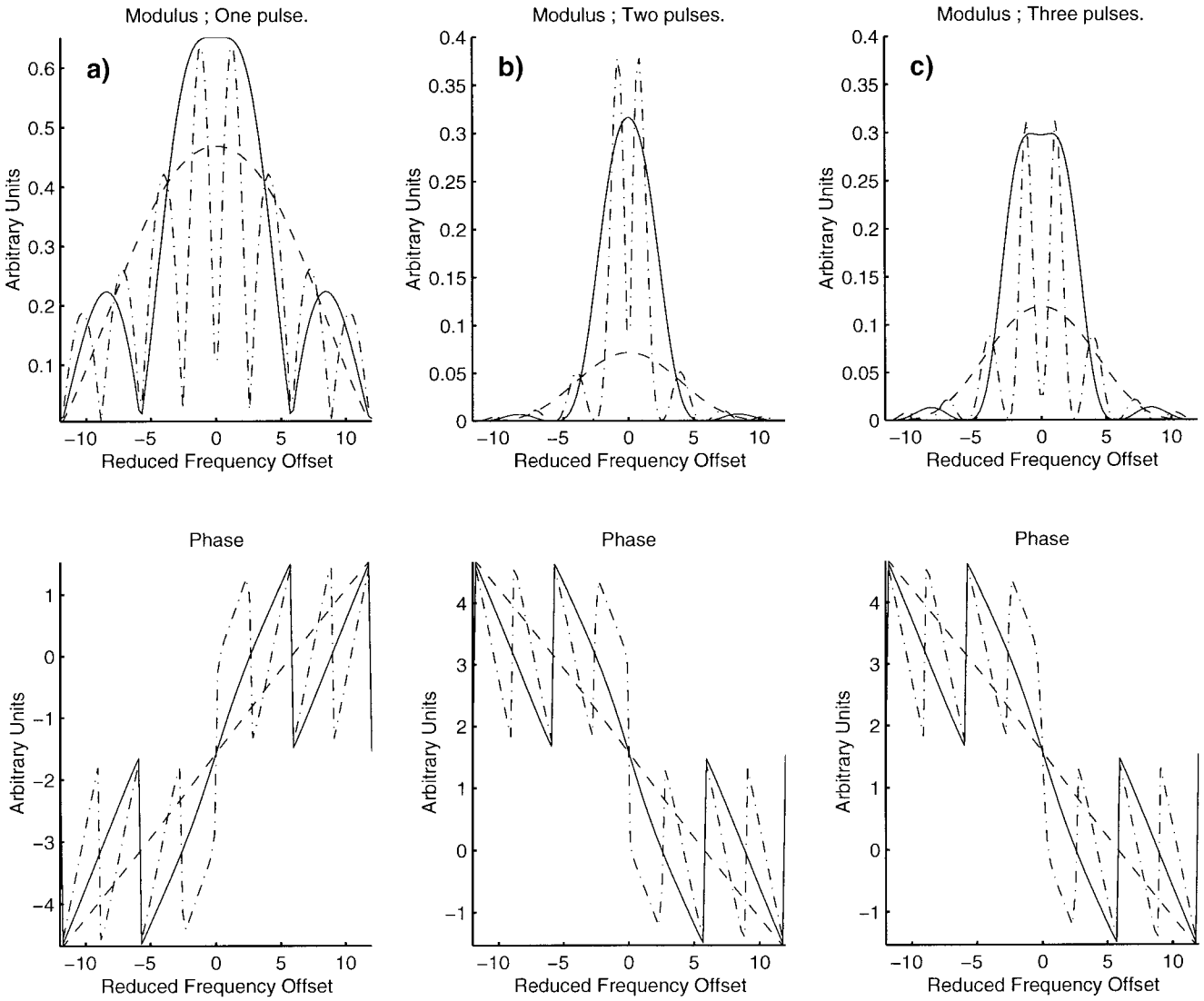

FIG. 9. Simulated modulus and phase of the excitation profiles as a function of irradiation frequency offset for different pulse angles $\theta = \omega_{RF}\, t_p$ ($\eta = 0.2$). (a) Sequence $\{\theta\}$; (b) sequence $\{\theta\}\ \{\theta\}$; (c) sequence $\{\theta\}\ \{\theta\}\ \{\theta\}$. Continuous line, $\theta = \theta_M$; dashed line, $\theta = \theta_M/2$; dash–dot line, $\theta = 2\theta_M$. The reduced frequency offset is $\Delta x = \Delta\omega/\omega_{RF}$.

of Table 4 indicates that the excitation bandwidth is limited by the longest pulse. Since the most favorable situation concerning the signal amplitude occurs when the first pulse is set to θ_M, the other pulse lengths could not exceed this value to keep a large excitation bandwidth. For this reason, we limited our study to the $\{\theta\}\ \{\theta\}$ and the $\{\theta\}\ \{\theta\}\ \{\theta\}$ "stimulated" echo sequences.

Figure 7 compares the excitation profile of different sequences as a function of frequency offset. The single pulse $\{\theta_M\}$ has obviously the largest bandwidth. Among all the echo sequences, the $\{\theta_M\}\ \{2\theta_M\}$ sequence gives obviously the smallest bandwidth, but the largest signal. The secondary maxima of sequences $\{\theta_M\}\ \{\theta_M\}$ and $\{\theta_M\}\ \{\theta_M\}\ \{\theta_M\}$ are almost unobservable, the last sequence giving a flatter profile than the $\{\theta_M\}\ \{\theta_M\}$ sequence. The Hahn-type sequence $\{\theta_M/2\}\ \{\theta_M\}$ is not recommended because it gives the weakest signal. Although not presented, we remark that the efficiency of $\{\theta\}\ \{\theta\}\ \{\theta\}$ is the best for a pulse angle set to $\theta = \theta_M$. If we draw a comparison between echo sequences having the same maximum pulse length, then the "stimulated echo" $\{\theta_M\}\ \{\theta_M\}\ \{\theta_M\}$ has the more uniform excitation profile.

These simulations were also compared to experimental data, keeping the same RF power value as in Fig. 4b, since all the experimental conditions were the same. Note that the data have *not* been corrected from the attenuation due to the resonant circuit. We found a very good agreement between the simulations and the experiment for all sequences, as indicated by Fig. 8.

An overestimation of the excitation bandwidth could be obtained by the first zero of the modulus of the response function in terms of the frequency offset. For a given λ' (which

means a given orientation when the sample is a monocrystal), the signal is zero at frequency offset

$$\frac{\Delta\nu_O}{\nu_{RF}} = \sqrt{\frac{1}{(2\nu_{RF}t_p)^2} - (\lambda')^2}. \quad [50]$$

For a powder sample, one must take into account the distribution of λ' and no evident solution was found. However, an approximate solution valid for low RF power can be obtained. Since the order of magnitude of parameter λ' is one ($\langle\lambda'\rangle \approx 1.4$), the first term in the root dominates λ' if $\nu_{RF} \ll 1/2\,t_p$. According to this approximation, the first zero is roughly independent of the RF power and of the powder average and is located at

$$\Delta\nu_0 \approx \pm\frac{1}{2t_p}. \quad [51]$$

If $t_p \approx 10\ \mu$s, then the maximum excitation bandwidth is $2\Delta\nu_0 \approx 100$ kHz and the RF power should be $\nu_{RF} \ll 50$ kHz. This approximation is usually valid. As a matter of fact, very low temperature experiments are usually performed under Helium gas, and very low RF powers are necessary to prevent arcing. For instance, the range of powers accessible with our spectrometer and probes without arcing are typically lower than 15 kHz. In the range of validity of this approximation, increasing the RF power only increases the magnitude of the secondary lobes of the excitation profile.

Considering the modulus of the signal is not sufficient, because the phase can only be corrected if it varies linearly with the frequency offset. An illustration of the effect of the pulse length on the excitation profile and phase linearity can be found on Fig. 9. Regardless of the pulse sequence, the range of linearity of the phase increases as the pulse angle decreases. When the pulse angle is set to $2\theta_M$ (giving an effective mean NQR π pulse), the signal amplitude vanishes at resonance, but off-resonance signal amplitude may be large.

CONCLUSION

Throughout this article, we tried to show that pure NQR of spin $I = \frac{3}{2}$ could be apprehended in a manner very similar to the framework of the high field NMR of an isolated single spin.

To draw this analogy, we explored the Q interaction representation formalism of an operator which is its own inverse and applied it to the pure NQR of spin $I = \frac{3}{2}$. This formalism greatly simplifies the cumbersome calculations given by Pratt in his pioneering article (*11*), by clearly pointing out the general properties of the transformed operators. For instance, only two parameters are needed, and only three matrices in the basis of the Cartesian operators had to be calculated. By means of this analogy with NMR, we were able to calculate the general propagator formula needed to calculate the response to every NQR multipulse sequence. A particular attention was devoted to the powder average, which was transformed from an average over a two-dimensional grid of angles to a one-dimensional average over the probability density of the angular factor, leading to a drastic decrease of simulation times. Moreover, the analytical expression of this probability density was derived, as well as the expressions of the corresponding nutation spectra. To our knowledge, this is the first time such an approach is applied to NQR and such analytical expressions are given.

Applications of these procedures to the study of the optimization and frequency response of one to three-pulse sequences were explicitly discussed and compared to some experiments performed on Chloranil. A three-pulse "stimulated echo" sequence allowing a flatter excitation profile than the traditional two-pulse echo sequences was proposed for powders and checked experimentally. A more general study of broadband pulse sequences will be the subject of another article.

APPENDIX A

We use the spin $\frac{1}{2}$ Pauli matrices, defined as

$$\sigma_z = \begin{pmatrix} 1 & 0 \\ 0 & -1 \end{pmatrix} \quad \sigma_x = \begin{pmatrix} 0 & 1 \\ 1 & 0 \end{pmatrix} \quad \sigma_y = \begin{pmatrix} 0 & -i \\ i & 0 \end{pmatrix}. \quad [A1]$$

Some well-known properties are

$$(\sigma_\alpha)^2 = I_2 \text{ and } \alpha = x, y, z. \quad [A2]$$

$$\sigma_x\sigma_y = i\sigma_z \text{ and the cyclic permutations} \quad [A3]$$

$$[\sigma_\alpha, \sigma_\beta]_+ = 0 \text{ and } \alpha \neq \beta. \quad [A4]$$

All calculations in the text are simplified by use of the following properties of the Kronecker product

$$(A \otimes B)(C \otimes D) = (AC) \otimes (BD) \quad [A5]$$

$$\mathrm{Tr}(A \otimes B) = \mathrm{Tr}(A)\mathrm{Tr}(B). \quad [A6]$$

APPENDIX B

In the basis which diagonalizes the quadrupolar Hamiltonian, the Q matrix is obviously represented by the following Kronecker product: $Q = \sigma_z \otimes I_2$.

Thus, if A is a 4×4 bloc matrix written as

$$A = \begin{pmatrix} a1 & a2 \\ a3 & a4 \end{pmatrix}, \quad [B1]$$

where ai are 2×2 matrices, one easily shows that the matrices r_A, p_A, and q_A are

$$r_A = \begin{pmatrix} a1 & 0 \\ 0 & a4 \end{pmatrix} \quad p_A = \begin{pmatrix} 0 & a2 \\ a3 & 0 \end{pmatrix} \quad q_A = -i\begin{pmatrix} 0 & -a2 \\ a3 & 0 \end{pmatrix}. \qquad [B2]$$

As a consequence, the matrices introduced by Pratt (*11*) could be retrieved by direct inspection of the matrix representation of the spin operators in the basis of the eigenfunctions of the quadrupolar Hamiltonian.

ACKNOWLEDGMENT

The author is particularly indebted to J. Gallier for fruitful discussions.

REFERENCES

1. K. Schmidt-Rohr and H. W. Spiess, "Multidimensional solid-state NMR and Polymers," Academic Press, San Diego (1994).
2. C. P. Slichter, "Principles of Magnetic Resonance," 3rd ed. Springer Verlag, Berlin (1990).
3. R. R. Ernst, G. Bodenhausen, and A. Wokaun, "Principles of Nuclear Magnetic Resonance in One and Two Dimension," Oxford Science Publications, Clarendon Press, London (1994).
4. J. C. Pratt, P. Raghunathan, and C. A. McDowell, Transient response of a quadrupolar spin system in zero applied field, *Mol. Phys.* **20,** 313–327 (1975).
5. R. Reddy and P. T. Narasimhan, Application of tensor operator formalism in pulsed nuclear quadrupole resonance spectroscopy, Part I: spin I = $\frac{3}{2}$ case in zero field, *Mol. Phys.* **72,** 491–507 (1991).
6. R. Reddy and P. T. Narasimhan, Application of tensor operator formalism in pulsed nuclear quadrupole resonance spectroscopy, Part II: spin I = $\frac{3}{2}$ case in a weak Zeeman field, *Mol. Phys.* **72,** 509–521 (1991).
7. M. Goldman, Spin-$\frac{1}{2}$ description of spins $\frac{3}{2}$, *Adv. Magn. Reson.* **14,** 59–74 (1990).
8. M. S. Krishnan, F. P. Temme, and B. C. Sanctuary, Theory of pulses in nuclear quadrupole resonance spectroscopy, I. Physical picture, *Mol. Phys.* **78,** 1385–1404 (1993).
9. S. Z. Ageev, D. J. Isbister, and B. C. Sanctuary, Composite pulses in nuclear quadrupole resonance, *Mol. Phys.* **83,** 193–210 (1994).
10. D. J. Isbister, M. S. Krishnan, and B. C. Sanctuary, Use of computer algebra for the study of quadrupole spin systems, *Mol. Phys.* **86,** 1517–1535 (1995).
11. J. C. Pratt, Nuclear quadrupole resonance in the interaction representation, *Mol. Phys.* **34,** 539–555 (1977).
12. S. Su and R. L. Armstrong, Bromine resonance in PrBr3 as an example of mixed spin echoes in pure nuclear quadrupole resonance, *J. Magn. Reson. Series A* **101,** 265–276 (1993).
13. G. S. Harbison, A. Slokenbergs, and T. M. Barbara, Two-dimensional zero-field nutation nuclear quadrupole resonance spectroscopy, *J. Chem. Phys.* **90,** 5292–5298 (1989).
14. H. Robert and D. J. Pusiol, One-dimensional nuclear quadrupole resonance spectroscopy for measurement of the electric field gradient tensor-asymmetry parameter, *J. Chem. Phys.* **106,** 2096–2100 (1997).
15. H. Robert, A. Minuzzi, and D. J. Pusiol, A fast method for the spatial encoding in rotating-frame NQR Imaging, *J. Magn. Reson. Series A* **118,** 189–194 (1996).
16. A. P. Bussandri and M. J. Zuriaga, Spin-echo mapping spectroscopy applied to NQR, *J. Magn. Reson.* **131,** 224–231 (1998).
17. P. Lancaster, "The Theory of Matrices," 2nd ed. Academic Press, New York (1985).
18. Gradstein, Ryshik, "Tables of Series, Products and Integrals," p. 294, Verlag Harri Deutzch (1981). We use the parameter $m = k^2$ for the definition of the complete elliptic integral of the first kind, that is $K(m) = K(k^2)$.